

Enhancing the thermal stability of entanglement between Majorana fermions with dipoles in optical lattices

Fei Lin and V.W. Scarola

Department of Physics, Virginia Tech, Blacksburg, Virginia 24061 USA

(Dated: October 3, 2012)

Pairing between spinless fermions can generate Majorana fermion excitations. Such excitations may exhibit intriguing properties arising from non-local entanglement, including anyonic braid statistics, teleportation, and enough stability to encode quantum information. But simple models indicate that non-local entanglement between Majorana fermions becomes unstable at non-zero temperatures. We address this issue here by showing that anisotropic interactions between dipolar fermions in optical lattices can be used to form domains that significantly enhance thermal stability. We construct a model of oriented dipolar fermions in a square optical lattice. We explicitly compute the correlation functions defining entanglement. We find that domains established by strong interactions exhibit enhanced entanglement between Majorana fermions over large distances and long times even at finite temperatures. Our approach can be generalized to a variety of configurations and other systems, such as quantum wire arrays.

Optical lattices offer unprecedented tunability in manipulating quantum degenerate gases into complex quantum states [1, 2]. The wide variety of lattice geometries accessible even allow enough control over anisotropy to explore dimensional crossover, for example between square and chain lattices. But recent developments in the cooling of molecules [3–8] and magnetic atoms [9] imply that a further level of anisotropy, anisotropy in inter-particle interactions, will be tunable in the near future. Such particles have dipolar interactions that, in combination with the wealth of lattice geometries possible, imply the ability to explore some of the most elusive yet compelling quantum states, entangled Majorana fermions.

Seminal lattice models demonstrate particle-like excitations that behave as Majorana fermions thanks to peculiar non-local symmetries [10, 11]. A Majorana fermion is its own antiparticle. But as excitations in many-body lattice models, they exploit symmetries with respect to operator strings that entangle with each other over large distances to signal underlying topological order, order that only responds to non-local perturbations such as the surface topology. Pairs of Majorana fermions entangled with string correlations support fascinating properties: The robustness of these strings motivated proposals for topologically protected qubits [11, 12]. The crossing of string operators is responsible for unusual anyonic braid statistics [11, 13]. And string operators connecting these excitations also underly theories of quantum state teleportation [14, 15].

The zero temperature properties of models hosting topological order set the stage for work connected to experiments. Kitaev's two dimensional toric code Hamiltonian [11] motivated early proposals in optical lattices containing ultracold atoms [16], polar molecules [17], and atoms in Rydberg states [18, 19]. But the one dimensional Kitaev chain model [10] is one of the simplest models supporting free Majorana fermion excitations. Antic-

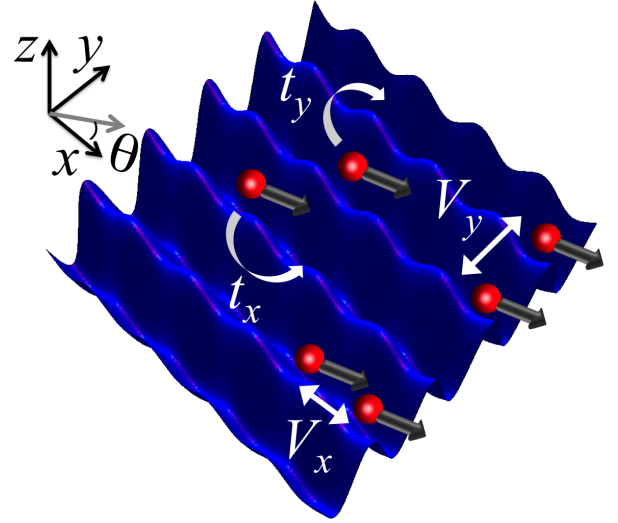


FIG. 1: Schematic of dipolar fermions (spheres) in the corrugated potential energy landscape defined by a two dimensional optical lattice. The arrows on each sphere indicate that the dipoles orient parallel to an applied field, at an angle θ with respect to the x -axis (grey arrow). The optical lattice imposes anisotropic hopping when the lattice depth is large along the y direction. The inter-fermion dipolar interaction is repulsive along the y direction, but attractive along the x direction for small θ .

ipation of non-local Majorana fermion properties in one dimension led to experimental proposals in both optical lattices [20–22] and solids [10, 23–26]. For example, proposals to observe Majorana fermions in quantum wires hosting a topological superconducting state lead to recent experiments that have shown promising results that can be interpreted as localized Majorana fermion excitations [27]. But prospects for observing interesting effects due to non-local entanglement of Majorana fermion pairs over long times and large length scales hinge on the sta-

bility of non-local string correlators [13] that have not yet been directly observed.

String correlation functions in simple Majorana fermion lattice models are unstable at non-zero temperatures. For example, direct calculations show that, in spite of a spectral gap, the string correlation functions supporting entangled Majorana fermions in Kitaev's two-dimensional toric code model vanish at long times and large distances because of thermally generated excitations [13, 28]. Recent work also argues that Majorana fermions in lattice models of topological p -wave superconductors are much more sensitive to thermal fluctuations than previously thought [29, 30]. A general theorem [28] shows that models of topological order must satisfy strict criteria for long-range entanglement to remain resilient against thermal fluctuations at long times. Fortunately, recent calculations [31, 32] show that proximity coupling [33] to a reservoir significantly helps in stabilizing topological superconductors in wires against thermal fluctuations [23–26].

We propose that spatially anisotropic dipolar interactions in optical lattices [34] offer a powerful tool to address the problem of thermodynamic stability of string correlators in lattice models of Majorana fermions. We argue that anisotropy in both the lattice and dipolar interactions can be used to electrostatically copy string correlations thus forcing excitations to form arrays of strings which we call *domains* in this work. We solve a simple model of dipolar atoms in an anisotropic square optical lattice with numerically exact quantum Monte Carlo (QMC) simulations to demonstrate that domain formation in electrostatically coupled Kitaev chains significantly enhances the built-in entanglement of string correlators. Our approach offers a powerful method to protect the long sought properties of Majorana fermions against thermal fluctuations at the level of the system to thereby complement proposals to stabilize Majorana fermions with reservoir coupling.

Model: We first consider a Hubbard model of dipolar fermions interacting in an optical lattice and then narrow our analysis to a specific parameter regime. Dipolar interactions can arise from an electric dipole moment in a polar molecule (e.g., $^{40}\text{K}^{87}\text{Rb}$ [5]) or an intrinsic magnetic dipole moment in a single atom (e.g., ^{161}Dy [9]). We assume that the dipoles orient along an applied external field (Fig. 1) but are allowed to hop between nearest neighbor (NN) sites. We also assume that a large optical lattice depth along the y direction strongly suppresses hopping in the y direction. We construct a Hubbard model capturing the essential features of this scenario:

$$H_D = - \sum_{i,j} \left(t_x a_{i,j}^\dagger a_{i+1,j} + t_y a_{i,j}^\dagger a_{i,j+1} + h.c. \right) + \sum_{i,j} [V_x(\theta) n_{i,j} n_{i+1,j} + V_y n_{i,j} n_{i,j+1} - \mu_0 n_{i,j}], \quad (1)$$

where we use $i = 1, 2, \dots, L_x - 1$ and $j = 1, 2, \dots, L_y$ to denote summation indices in the x and y directions, respectively. $a_{i,j}^\dagger$ creates a spinless fermion at the site (i, j) and $n_{i,j} = a_{i,j}^\dagger a_{i,j}$ is the particle number operator. $t_x(t_y)$ is the hopping energy between NN sites in the $x(y)$ direction. The chemical potential, μ_0 , controls the average density. Our approach will work in many different lattice geometries of different dimensions but to demonstrate an example, electrostatically coupled Kitaev chains, we consider the square lattice with $L = L_x = L_y$. (The supplementary information section discusses boundary conditions used in calculations.)

The interaction terms capture the short-range Hubbard part of the dipolar interaction. We will focus on limits with an energy gap and can therefore truncate the interaction to NN sites provided that renormalization from the long-range part of the interaction yields corrections that are much smaller than the gap. We approximate the Hubbard parameters with their bare values. The dipolar interaction between NN sites in the x and y direction is given by $V_x(\theta) = D^2(1 - 3\cos^2\theta)/r_0^3$ and $V_y = D^2/r_0^3$, respectively. Here $r_0 = \lambda/2$ is the lattice constant defined by the optical lattice laser wavelength, λ . In the case of electric dipoles, $D^2 = \vec{p}^2/4\pi\epsilon_0$ with ϵ_0 the dielectric constant and \vec{p} the electric dipole moment. Rotation of an applied external field with respect to the optical lattice plane tunes the angle that the dipoles make with the x -axis, θ . We consider angles such that the fermions are attractive along the x -rows (rows along the x direction in the optical lattice), $V_x < 0$, but repulsive along y -columns (columns along the y direction in the lattice), $V_y > 0$.

For a range of θ yielding $V_x < 0$ the ground state of Eq. (1) exhibits p -wave pairing. For $t_x = t_y$ functional renormalization group [35] and mean-field [36, 37] calculations show a BCS paired state for dipolar interactions consistent with Eq. (1) [29]. p -wave pairing between neighbors along x -rows can be modeled by a real space pairing field: $\exp(i\Phi_{i,j})|\Delta|(a_{i+1,j}^\dagger a_{i,j}^\dagger + a_{i,j} a_{i+1,j})$. But in the $t_y \ll t_x$ limit the system can be thought of as weakly coupled Luttinger liquids in x -rows. A Luttinger liquid theory analysis shows that weakly coupled 1D dipolar systems also possess p -wave paired order with algebraic decaying pairing correlations [38]. Increasing t_y connects the coupled-1D and 2D square lattice limits.

t_y establishes a Josephson coupling between x -rows. In the limit that the inter- x -row tunneling is much smaller than the pairing gap within an x -row, we expect second order tunneling between paired states: $\sim -t_y^2 \cos(\Phi_{i,j} - \Phi_{i,j+1})$. Because the system is otherwise insensitive to changes in the relative phase between chains, the Josephson coupling will tend to align the phase of the pairing field between each x -row, $\Phi_{i,j} - \Phi_{i,j+1} \rightarrow 0$. In what follows we assume a uniform pairing field to motivate a model that allows the identification of domains of Majorana

rana fermion strings with significantly enhanced thermal stability. We then discuss corrections in the pair field due to fluctuations.

Mean-Field Limit: We perform a mean-field decoupling of Eq. (1) to establish a more general model. We take t_y to be energetically negligible. By decoupling just the attractive dipolar interaction term in the x direction we find:

$$H_F = -t \sum_{i,j} \left(a_{i,j}^\dagger - a_{i,j} \right) \left(a_{i+1,j}^\dagger + a_{i+1,j} \right) + V_y \sum_{i,j} \left(n_{i,j} - \frac{1}{2} \right) \left(n_{i,j+1} - \frac{1}{2} \right) - \mu \sum_{i,j} n_{i,j}. \quad (2)$$

At the Hartree-Fock level the chemical potential is renormalized to $\mu = \mu_0 + 2\langle n_{i,j} \rangle |V_x| - \frac{1}{2}V_y$ and the hopping becomes $t = t_x - |V_x(\theta)| \langle a_{i+1,j}^\dagger a_{i,j} \rangle$. In Eq. (2), we, without loss of generality, tuned θ to match the renormalized pairing term with the hopping by setting $t_x = |V_x(\theta)| \langle a_{i+1,j}^\dagger a_{i,j}^\dagger + a_{i+1,j}^\dagger a_{i,j} \rangle$. Majorana fermions can arise away from this particular point in parameter space but this choice eliminates the fermion sign problem in our model. This choice also implicitly includes the second order effect of the t_y term by setting $\Phi_{i,j} = 0$ in the pairing field. t is our energy unit.

Eq. (2) establishes a parameterization of the dipolar problem that forms the centerpiece of our work. We will use both mean field theory (MFT) and QMC on this model to explicitly demonstrate the robustness of domains against thermal fluctuations. We choose $\mu = 0$ (unless stated otherwise) to work near fillings with an average of one particle for every two sites. At this filling our findings also apply to $V_y < 0$, since both cases are equivalent under a particle-hole transformation on one sublattice.

Eq. (2) reduces to known models in certain limits. For $t/V_y = 0$ the model does not support kinetics. The ground state is essentially a classical state of independent one-dimensional charge density waves aligned along y -columns. In the opposite limit, $t/V_y \rightarrow \infty$, we find a series of one dimensional Kitaev chains oriented along x -rows. For $V_y = 0$ these x -rows can be mapped onto a model of free Majorana fermions. It is known that interactions within one or two chains can increase the gap [39, 40]. But by coupling these chains with strong interactions, $V_y > 4t$, we will show below that Majorana fermions form in unison along columns, to offer a qualitatively more robust mechanism for enhancing entanglement between entire y -columns of Majorana fermions.

Mapping to Majorana Fermions: We can transform the above interacting spinless fermion Hamiltonian into an interacting Majorana fermion model by introducing two Majorana fermion operators, $c_{2i,j}$ and $c_{2i-1,j}$, for each site of the lattice, (i,j) [10]. These operators satisfy the usual fermion anticommutation relations: $c_{\alpha,\beta} c_{\alpha',\beta'} =$

$-c_{\alpha',\beta'} c_{\alpha,\beta}$, for $\{\alpha,\beta\} \neq \{\alpha',\beta'\}$. But these particles are also their own antiparticle: $c_{\alpha,\beta} = c_{\alpha,\beta}^\dagger$ and $(c_{\alpha,\beta})^2 = 1$. The absence of kinetics along the y direction implies that each particle can be labeled with a specific x -row index, j . The Majorana fermion operators then relate to the physical fermion operators by a complex superposition:

$$a_{i,j} = (c_{2i-1,j} + i c_{2i,j})/2 \\ a_{i,j}^\dagger = (c_{2i-1,j} - i c_{2i,j})/2. \quad (3)$$

We can now demonstrate the existence of edge states by mapping Eq. (2) to Majorana fermion space:

$$H_M = i t \sum_{i,j} c_{2i,j} c_{2i+1,j} + \frac{i\mu}{2} \sum_{i,j} c_{2i-1,j} c_{2i,j} - \frac{V_y}{4} \sum_{i,j} c_{2i-1,j} c_{2i,j} c_{2i-1,j+1} c_{2i,j+1}. \quad (4)$$

Here we see that the first two terms equate to the Kitaev chain [the first two terms in Eq. (2)] and define a free Majorana fermion theory. States defined by the dangling operators, $c_{1,j}$ and $c_{2L_x,j}$, at the ends of each x -row establish two-fold degenerate Majorana fermion states that can be entangled at $T = 0$. By *non-local entanglement* we mean that this operator pair hosts a single real dipole in a superposition of states that stretches across the j^{th} x -row.

The Hilbert space of Eq. (2) also maps onto a quantum compass model which possesses a spectral gap, ΔE , above the degenerate states for the parameters we consider here [41, 42]. But the entropy gain in the free energy cost to create excitations, $\Delta E - k_B T S$, can overwhelm the energy gap in low dimensions. Here S is the entropy and k_B is Boltzmann's constant.

The thermal stability of entanglement among excitations depends on the ratio V_y/t . For weak interactions, $V_y < 4t$, the system can be thought of as nearly independent one-dimensional x -rows of free Majorana fermions. Non-zero T allows the accumulation of entropy through the proliferation of Majorana fermion pairs to destroy entanglement at long times and large distances (since $\Delta E \sim \mathcal{O}(1)$ and $S \sim \ln L_x$) even though fluctuations in the pairing field are ignored. But we argue that strong interaction between x -rows, $V_y > 4t$, significantly improves the thermal stability of entanglement between edge states because they extend along y -columns. Strong interactions therefore require the creation of entire domains (with $\Delta E \sim L_y$ and $S \sim \ln L_x$) to destroy entanglement. [The domain picture is exact in a mean field limit that is shown to be an excellent approximation to Eq. (2) in the supplementary information section.] We thus propose that the interesting entanglement properties between y -columns of Majorana fermions are much more thermodynamically stable than those between pairs of individual Majorana fermions.

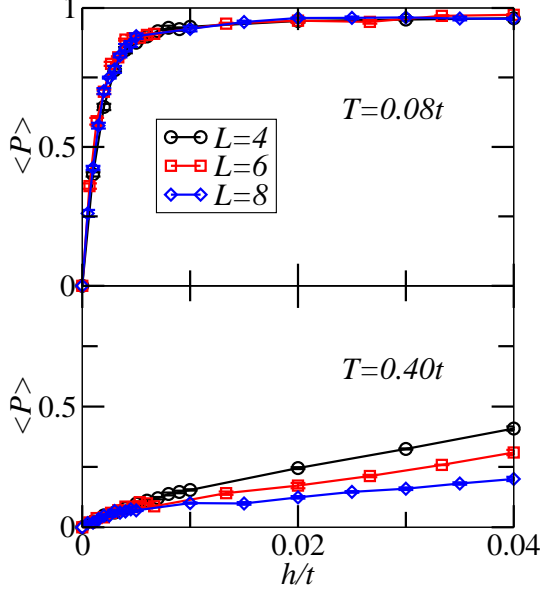


FIG. 2: The thermal expectation value of the string operator plotted as a function of an applied global field [defined in Eq. (6)] for several different system sizes, L , at $V_y = 4.8t$ and $\mu = 0$, computed using QMC. The string operator can only be ± 1 at $T = 0$ but may vanish for $T > 0$. The top (bottom) panel shows data for a characteristic low (high) temperature. In the top panel we see that very small values of h tend to polarize each x -row of the two dimensional lattice into the same parity sector, $+1$. The data collapse and very small h values suggest that the parity symmetry of each x -row is spontaneously broken. The bottom panel shows that at high T , large fields are required to occupy the $+1$ sector.

Thermal Stability of Majorana Fermion Entanglement: The degree of entanglement between edge states prepared at $i = 1$ and $i = L_x$ is captured by a set of L_y string operators that stretch across each x -row:

$$P_j \equiv \prod_{i=1}^{L_x} (1 - 2n_{i,j}) = (-1)^{\sum_i n_{i,j}}, \quad (5)$$

where $j = 1, 2, \dots, L_y$ along the y direction. The second equality shows that this operator is equivalent to the fermion parity for each x -row. Each operator P_j has two eigenvalues, ± 1 . P_j commutes with Eq. (2) to establish a 2^{L_y} degeneracy [41, 42] on our geometry of choice, the cylinder.

The expectation value of the string operators, P_j , act as order parameters. Unique values, $\langle P_j \rangle = \pm 1$, can be used to define each sector and therefore indicate stability in the non-local entanglement of Majorana fermions. But $\langle P \rangle = 0$ indicates that thermal excitations destroy any distinction between sectors. We compute $\langle P_j \rangle$ ex-

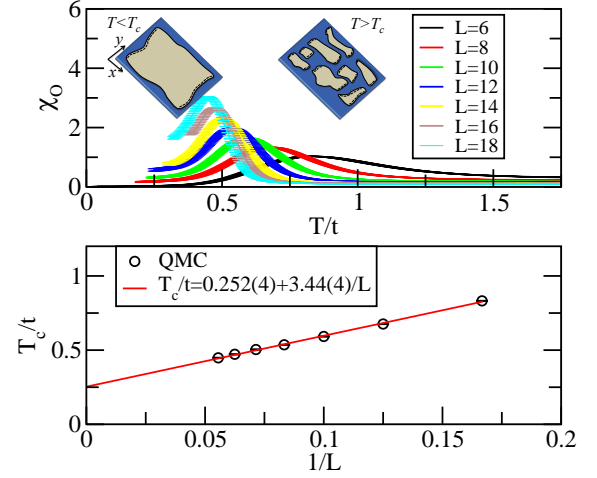


FIG. 3: Top: The susceptibility of the string-string correlation function, Eq. (7), computed using QMC on Eq. (2) for several different system sizes at $V_y = 4.8t$ and $\mu = 0$. T_c is defined as the location of the susceptibility peak. The string operators tend to order along the y direction for $T < T_c$. The inset shows a schematic of an ordered domain with free Majorana fermions forming columns at the ends (dashed lines). The domains shrink for $T > T_c$. Bottom: T_c extrapolated to $L \rightarrow \infty$. The solid line is a straight line chi-squared fit indicating non-zero T_c in the thermodynamic limit.

plicitly to show spontaneous breaking of these discrete symmetries for $V_y > 4t$ even at non-zero temperatures. To detect the spontaneous breaking of the string symmetries we perturb the above spinless fermion model with a weak global field:

$$H = H_F - \tilde{h} \sum_{j=1}^{L_y} P_j. \quad (6)$$

The global field, $P = L_y^{-1} \sum_{j=1}^{L_y} P_j$, imposes a splitting between the otherwise degenerate states. We define $\tilde{h} = hL_x$ with the factor L_x to ensure that the perturbing term imposes a non-zero energy splitting per particle, h , between degenerate sectors even in the limit $L_x = L_y \rightarrow \infty$. $h > 0$ favors uniform P_j , $\langle P \rangle = 1$.

We first compute $\langle P \rangle$ in the limit $V_y < 4t$ using QMC. The expectation value is computed using the quantum Wang-Landau algorithm in the stochastic series expansion representation [43, 44] (this unbiased method is numerically exact and is discussed in the supplementary information section). For $V_y = 0.04t$ we find $\langle P \rangle \approx 0$ to within numerical accuracy for $h < 0.02t$, $T = 0.08t$, and $L = 4-8$. For $V_y = 3.2t$ we find $\langle P \rangle \rightarrow 0$ with increasing L . This indicates that the operators defining the sectors in one dimensional x -rows alone are extremely sensitive

to thermal fluctuations even for small system sizes, as expected from the entropy argument above. We note that our calculations are time independent. It is possible that one can find $|\langle P \rangle| > 0$ at short times for weak interactions.

We now turn to calculations of $\langle P \rangle$ in the strongly interacting case, $V_y = 4.8t$, where we expect arrays of strings to form stable domains. Fig. 2 shows $\langle P \rangle$ at low and high temperatures computed using Eq. (6). Fig. 2 presents the central result of our work. At high T the bottom panel shows that a large value of h is needed to stabilize the string operator. But at low T (top panel) we find that very small fields tend to force all x -rows to spontaneously occupy the lowest energy state in the limit $h \rightarrow 0$. (We do not find this behavior for $V_y < 4t$.) The top panel indicates that y -columns of Majorana fermions located at the ends of the lattice, $i = 1$ and $i = L_x$, can be prepared in a long lasting entangled state, that stretches over large distances, even at finite temperatures.

Thermal Stability of Domains: The arrays of string operators defining domains are stable at low temperatures but eventually break up at large T . To find the critical temperature at which domain formation becomes unfavorable, we define a string-string order parameter that captures the strength of the ordering along the y direction:

$$\langle O \rangle \equiv \frac{1}{L_y^2} \sum_{j,j'=1}^{L_y} \langle P_j P_{j'} \rangle. \quad (7)$$

The operator O is similar to the static structure factor, $S_{k_y} \propto \sum_{j,j'=1}^{L_y} \exp[-ik_y(j-j')] \langle n_j n_{j'} \rangle$, but with the replacement $n_j n_{j'} \rightarrow P_j P_{j'}$ and with wavevector $k_y = 0$. Thus, the ordering of the string operators along the y direction is picked out by the operator O in a way analogous to definitions of density-ordering using peaks in the static structure factor.

We look for long-range order in the susceptibility of O , χ_O . A peak in χ_O versus T indicates the critical temperature T_c at which the large domain breaks up along the y direction. For $V_y < 4t$ we find no peaks in our simulations and therefore no domain formation for weakly interacting chains, i.e., $T_c = 0$.

We observe domain formation in χ_O for $V_y > 4t$. The top panel of Fig. 3 shows the susceptibility of O computed using Eq. (2) as a function of temperature for $V_y = 4.8t$. Above T_c the y -columns of Majorana fermions are no longer ordered and the average domain size shrinks. At these high temperatures the system can be thought of as a thermally disordered phase of ordinary fermions. The peak also shifts with system size. The bottom panel extracts T_c in the thermodynamic limit, yielding $T_c = 0.25t$. Our results agree with studies showing a thermal phase transition in the universality class of the two dimensional Ising model [45].

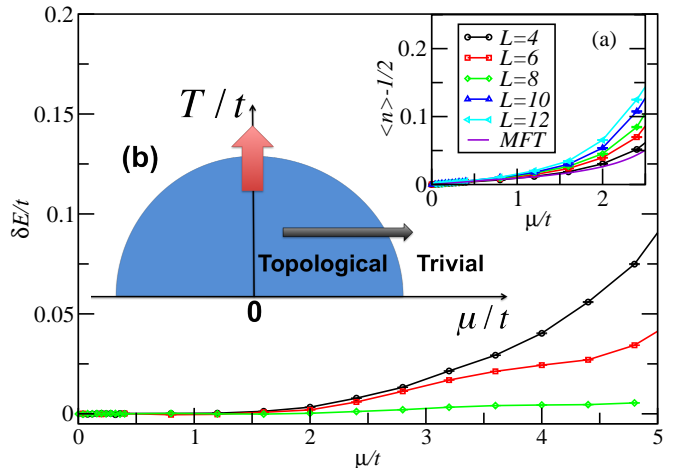


FIG. 4: The main panel plots the energy splitting between two sectors defined by $P_j = \pm 1$ for all x -rows as a function of chemical potential for Eq. (2) at $T = 0.16t$ and $V_y = 4.8t$. For weak chemical potentials the degeneracy remains robust but an L dependent splitting arises for large chemical potentials. Inset (a) shows a weak linear increase in density with increasing chemical potential. The $\mu \rightarrow 0$ slope is quantitatively captured by mean field theory. Inset (b) shows a schematic phase diagram established by the lifting of the degeneracy, horizontal arrow. The vertical arrow indicates the thermal phase transition explored in Fig. 3.

The robustness of the ground state degeneracy also reveals the stability of the string correlations. We denote each ground state energy sector by $E(P_1, P_2, \dots)$. We attempt to perturb this degeneracy with a local field, a chemical potential shift, to demonstrate the stability of the degeneracy that is enforced by the spectral gap. The main panel of Fig. 4 shows the energy splitting per particle of two different sectors of the P_j operator computed with Eq. (2): $\delta E \equiv E(-1, -1, \dots) - E(1, 1, \dots)$, as a function of chemical potential. The flat portion for $\mu/t \ll 1$ indicates a robust degeneracy. Above $\mu \approx 1.5t$ the energy splitting acquires a size dependence consistent with behavior expected for chemical potentials above the gap. Inset (a) shows that the particle density has weak linear dependence for $\mu/t \ll 1$ which is also captured by the MFT discussed in the supplementary information section. Our results are consistent with the formation of a thermally robust topological phase at $T > 0$, shown in inset (b) of Fig. 4.

Detection in Optical Lattices: Domain formation can be observed directly in time-of-flight measurements. Noise correlations between shots of individual time-of-flight images relate to the static structure factor, S_k , of optical lattice states [46]. Peaks in noise correlations have already been used to identify uniform states in optical lattices [47, 48]. In the topological phase with domains we anticipate the formation of lines, rather than peaks, in noise correlations because the density oscillates along just

the y direction of the optical lattice for $T < T_c$. Observations of these lines should therefore allow identification of T_c .

Entanglement between Majorana fermions could be demonstrated through non-local measures. A trapping potential, modeled by a spatially varying μ , will allow the topological phase near the center of the trap to remain intact. But it will leave a topologically trivial phase near the edges [large negative μ in inset (b) of Fig. 4]. A dipole added to one domain edge should instantaneously occupy a superposition of both edge states. Local spectroscopic probes (see, e.g., Refs. [20, 22]) applied at each domain edge could be adapted to detect the response of one domain edge when dipoles are added to the opposite edge. Analogous teleportation experiments have been proposed in the solid state [14, 15]. But ultracold atoms offer more direct methods. Recent experiments using high resolution spectroscopy to measure particle number parity [49] and string operators [50] could be used to explicitly measure the string correlation functions, $\langle P_j \rangle$, for domains near the trap center and therefore directly detect long-range entanglement.

Thermal Fluctuations in Pairing: We connected a model of oriented fermionic dipoles placed in optical lattices, Eq. (1), to a pairing model, Eq. (2). The pairing model itself demonstrates significantly enhanced stability of Majorana fermion entanglement (captured by $\langle P \rangle$) via domain formation at $T > 0$. But our specific implementation allows thermal fluctuations of a different quantity, the pairing field, $\exp(i\Phi_{i,j})|\Delta|$, between x -rows. The long range component of the dipolar interaction has been found to enhance the thermal stability of p -wave superfluidity [37] but other mechanisms can be engineered to further enhance stability.

Coherent reservoirs can be constructed to suppress fluctuations of the pairing field within the system. Several schemes for inducing a pairing field have been proposed to generate Majorana fermion models with, e.g., dissipation-induced pairing [21] or coupling to a reservoir of bosons [22]. These schemes can be adapted to ensure pairing fields in dipolar systems. Another alternative could use the proximity effect of a reservoir dipolar superfluid to stabilize the pairing field in the system discussed here [33]. The pairing gap in the reservoir would favor pair tunneling, for weak single-particle tunneling between the reservoir and the system, to strengthen the pairing field throughout the system. (The supplementary information section discusses a candidate optical lattice geometry defining a system and reservoir.) Care must be taken in engineering the reservoir because excitations in the system can be strongly coupled to excitations in the reservoir [31, 32].

Discussion: We have constructed a mechanism to enhance Majorana Fermion entanglement in an anisotropic lattice model. Our approach generalizes to a variety of lattice geometries and even other models with

Majorana fermions provided they take a similar form: $\sum_a H_M^a + \sum_{a,b} V_{\text{int}}^{a,b}$, where H_M^a defines a model with Majorana fermions, $V_{\text{int}}^{a,b}$ creates domains with diagonal interactions between models a and b , and $V_{\text{int}}^{a,b}$ does not commute with H_M^a [28]. This class of Hamiltonians also applies to Coulomb-coupling in Majorana fermion models of quantum wire arrays or quasi-1D tubes containing topological superconductors.

We thank R. Lutchyn, S. Tewari, M. Troyer, and C. Zhang for helpful discussions. We acknowledge support from the ARO(62366PHII), AFOSR (FA9550-11-1-0313), and DARPA-YFA (N66001-11-1-4122). Some of the calculations were performed at the Lonestar cluster in the Texas Advanced Computing Center at the University of Texas at Austin.

-
- [1] Greiner, M., Mandel, O., Esslinger, T., Hansch, T. W., and Bloch, I., Quantum phase transition from a superfluid to a Mott insulator in a gas of ultracold atoms. *Nature* **415**, 39 (2002).
 - [2] Bloch, I., Dalibard, J., and Zwerger, W., Many-body physics with ultracold gases. *Rev. Mod. Phys.* **80**, 885 (2008).
 - [3] Ospelkaus, S. *et al.*, Efficient state transfer in an ultracold dense gas of heteronuclear molecules. *Nat. Phys.* **4**, 622 (2008).
 - [4] Voigt, A. C. *et al.*, Ultracold heteronuclear Fermi-Fermi molecules. *Phys. Rev. Lett.* **102**, 020405 (2009).
 - [5] Ni, K. K. *et al.*, Dipolar collisions of polar molecules in the quantum regime. *Nature* **464**, 1324 (2010).
 - [6] Chotia, A. *et al.*, Long-lived dipolar molecules and Feshbach molecules in a 3D optical lattice. *Phys. Rev. Lett.* **108**, 080405 (2012).
 - [7] Heo, M. S. *et al.*, Formation of Ultracold Fermionic NaLi Feshbach Molecules. arXiv:1205.5304.
 - [8] Wu, C., Park, J. W., Ahmadi, P., Will, S., and Zwierlein, M. W., Ultracold Fermionic Feshbach Molecules of $^{23}\text{Na}^{40}\text{K}$. *Phys. Rev. Lett.* **109**, 085301 (2012).
 - [9] Lu, M., Burdick, N. Q., and Lev, B. L., Quantum, degenerate dipolar Fermi gas. *Phys. Rev. Lett.* **108**, 215301 (2012).
 - [10] Kitaev, A. Y., Unpaired Majorana fermions in quantum wires. *Phys.-Usp.* **44**, 131 (2001).
 - [11] Kitaev, A. Y., Fault-tolerant quantum computation by anyons. *Ann. Phys.* **303**, 2 (2003).
 - [12] Nayak, C., Simon, S. H., Stern, A., Freedman, M., and Das Sarma, S., Non-Abelian anyons and topological quantum computation. *Rev. Mod. Phys.* **80**, 1083 (2008).
 - [13] Nussinov, Z. and Ortiz, G., A symmetry principle for topological quantum order. *Ann. Phys.* **324**, 977 (2009).
 - [14] Semenov, G. W. and Sodano, P., Stretched quantum states emerging from a Majorana medium. *J. Phys. B: At. Mol. Opt. Phys.* **40**, 1479 (2007).
 - [15] Tewari, S., Zhang, C., Das Sarma, S., Nayak, C., Lee, D. H., Testable Signatures of Quantum Nonlocality in a Two-Dimensional Chiral p -Wave Superconductor. *Phys. Rev. Lett.* **100**, 027001 (2008).
 - [16] Duan, L. M., Demler, E., and Lukin, M. D., Controlling

- spin exchange interactions of ultracold atoms in optical lattices. *Phys. Rev. Lett.* **91**, 090402 (2003).
- [17] Micheli, A., Brennen, G. K., and Zoller, P., A toolbox for lattice-spin models with polar molecules. *Nat. Phys.* **2**, 341 (2006).
- [18] Weimer, H., Müller, M., Lesanovsky, I., Zoller, P., and Büchler, H. P., A Rydberg quantum simulator. *Nat. Phys.* **6**, 382 (2010).
- [19] Herdman, C. M., Young, K. C., Scarola, V. W., Sarovar, M., and Whaley, K. B., Stroboscopic generation of topological protection. *Phys. Rev. Lett.* **104**, 230501 (2010).
- [20] Jiang, L. *et al.*, Majorana fermions in equilibrium and in driven cold-atom quantum wires. *Phys. Rev. Lett.* **106**, 220402 (2011).
- [21] Diehl, S., Rico, E., Baranov, M. A., and Zoller, P., Topology by Dissipation in Atomic Quantum Wires. *Nat. Phys.* **7**, 971 (2011).
- [22] Kraus, C. V., Diehl, S., Zoller, P., and Baranov, M. A., Probing atomic Majorana fermions in optical lattices. arXiv:1201.3253.
- [23] Alicea, J., Oreg, Y., Refael, G., von Oppen, F., and Fisher, M. P. A., Non-Abelian statistics and topological quantum information processing in 1D wire networks. *Nat. Phys.* **7**, 412 (2011).
- [24] Lutchyn, R. M., Sau, J. D., and Das Sarma, S., Majorana Fermions and a Topological Phase Transition in Semiconductor-Superconductor Heterostructures. *Phys. Rev. Lett.* **105**, 077001 (2010).
- [25] Oreg, Y., Refael, G., and von Oppen, F., Helical liquids and Majorana bound states in quantum wires. *Phys. Rev. Lett.* **105**, 177002 (2010).
- [26] Mao, L., Gong, M., Dumitrescu, E., Tewari, S., and Zhang, C., Hole-doped semiconductor nanowire on top of an s-wave superconductor: A new and experimentally accessible system for Majorana fermions. *Phys. Rev. Lett.* **108**, 177001 (2012).
- [27] Mourik, V. *et al.*, Signatures of Majorana fermions in hybrid superconductor-semiconductor nanowire devices. *Science* **336**, 1003 (2012).
- [28] Hastings, M. B., Topological order at nonzero temperature. *Phys. Rev. Lett.* **107**, 210501 (2011).
- [29] Cheng, M., Sun, K., Galitski, V., and Das Sarma, S., Stable topological phases in a family of two-dimensional fermion models. *Phys. Rev. B* **81**, 024504 (2010).
- [30] Bauer, B., Lutchyn, R. M., Hastings, M. B., and Troyer, M., Effect of thermal fluctuations in topological p-wave superconductors. arXiv:1206.1326.
- [31] Fidkowski, L., Lutchyn, R. M., Nayak, C., and Fisher, M. P. A., Majorana Zero Modes in 1D Quantum Wires Without Long-Ranged Superconducting Order. *Phys. Rev. B* **84**, 195436 (2011).
- [32] Sau, J. D., Halperin, B. I., Flensberg, K., and Das Sarma, S., A number conserving theory for topologically protected degeneracy in one-dimensional fermions, *Phys. Rev. B* **84**, 144509 (2011).
- [33] Fu, L. and Kane, C. L., Superconducting Proximity Effect and Majorana Fermions at the Surface of a Topological Insulator. *Phys. Rev. Lett.* **100**, 096407 (2008).
- [34] Baranov, M. A., Dalmonte, M., Pupillo, G., and Zoller, P., Condensed Matter Theory of Dipolar Quantum Gases. *Chemical Reviews* **112**, 5012 (2012).
- [35] Bhongale, S. G., Mathey, L., Tsai, S., Clark, C. W., and Zhao, E., Bond order solid of two-dimensional dipolar fermions. *Phys. Rev. Lett.* **108**, 145301 (2012).
- [36] Gadsbølle, A. and Bruun, G. M., Harmonically trapped dipolar fermions in a two-dimensional square lattice. *Phys. Rev. A* **85**, 021604(R) (2012).
- [37] Liu, B. and Yin, L., Topological $p_x + ip_y$ Superfluid Phase of a Dipolar Fermi Gas in a 2D Optical Lattice. *Phys. Rev. A* **86**, 031603(R) (2012).
- [38] Huang, Y. P. and Wang, D. W., Quantum phase diagrams of fermionic dipolar gases for an arbitrary orientation of dipole moment in a planar array of 1D tubes. *Phys. Rev. A* **80**, 053610 (2009).
- [39] Stoudenmire, E. M., Alicea, J., Starykh, O. A., and Fisher, M. P. A., Interaction effects in topological superconducting wires supporting Majorana fermions. *Phys. Rev. B* **84**, 014503 (2011).
- [40] Lutchyn, R. M. and Fisher, M. P. A., Interacting topological phases in multiband nanowires. *Phys. Rev. B* **84**, 214528 (2011).
- [41] Chen, H., Fang, C., Hu, J., and Yao, H., Quantum phase transition in the quantum compass model. *Phys. Rev. B* **75**, 144401 (2007).
- [42] Dorier, J., Becca, F., Mila, F., Quantum compass model on the square lattice. *Phys. Rev. B* **72**, 024448 (2005).
- [43] Syljuåsen, O. F. and Sandvik, A. W., Quantum Monte Carlo with directed loops. *Phys. Rev. E* **66**, 046701 (2002).
- [44] Troyer, M., Wessel, S., and Alet, F., Flat Histogram Methods for Quantum Systems: Algorithms to Overcome Tunneling Problems and Calculate the Free Energy. *Phys. Rev. Lett.* **90**, 120201 (2003).
- [45] Wenzel, S. and Janke, W., Monte Carlo simulations of the directional-ordering transition in the two-dimensional classical and quantum compass model. *Phys. Rev. B* **78**, 064402 (2008).
- [46] Altman, E., Demler, E., and Lukin, M. D. Probing many-body states of ultracold atoms via noise correlations. *Phys. Rev. A* **70**, 013603 (2004).
- [47] Foelling, S. *et al.*, Spatial quantum noise interferometry in expanding ultracold atom clouds. *Nature* **434**, 481 (2005).
- [48] Spielman, I. B., Phillips, W. D., and Porto, J. V., Topological order at nonzero temperature. *Phys. Rev. Lett.* **98**, 080404 (2007).
- [49] Simon, J. *et al.*, Quantum simulation of antiferromagnetic spin chains in an optical lattice. *Nature* **472**, 307 (2011).
- [50] Endres, M. *et al.*, Observation of correlated particle-hole pairs and string order in low-dimensional Mott insulators. *Science* **334**, 200 (2011).

SUPPLEMENTARY MATERIAL

Monte Carlo Method and Simulation Parameters

We use quantum Monte Carlo (QMC) to solve the spinless fermion model, Eq. (2), by first using a Jordan-Wigner transformation to map the model onto the quantum compass model [1]. We then perform simulations implemented with the Stochastic Series Expansion (SSE) [2] combined with the quantum Wang-Landau algorithm [3]. In this approach the partition function is expanded

as a series in powers of $\beta \equiv (k_B T)^{-1}$:

$$Z = \text{Tr} e^{-\beta H} = \sum_{n=0}^{N_{\max}} \frac{\beta^n \text{Tr}(-H)^n}{n!} = \sum_{n=0}^{N_{\max}} g(n) \beta^n, \quad (8)$$

where N_{\max} is the maximum cutoff of the expansion order. N_{\max} determines the lowest temperature that can be reached in the simulation, and $g(n)$ corresponds to the density of states in a classical system. The distribution of $g(n)$ is obtained from a random sampling protocol [3] and can be used to estimate the free energy, internal energy, entropy, heat capacity, and other properties of the system. Note, to measure other physical quantities such as the density, density-density correlation, and the string operator, we need to accumulate their distribution at every order of the series expansion.

There is a very large energy barrier between different sectors defined by the P operator. The large energy barrier dramatically increases the autocorrelation time in conventional QMC simulations with non-local updating. Therefore, to reduce the autocorrelation time in QMC and enable tunneling between different P sectors, implementation of the Wang-Landau algorithm is necessary to accurately access the phases discussed in the paper.

We find that cylindrical boundary conditions (periodic in the y direction) are the best choice for this particular model. The one dimensional quantum Ising model [which can be related to Eq. (2) in the limit $V_y = 0$ after a Jordan-Wigner transformation] loses the two-fold ground state degeneracy in finite sized systems under periodic boundary conditions [4, 5]. The degeneracy remains exact in finite sized systems under open boundary conditions [4, 5]. The corrections in periodic boundaries relate to the fact that the quantum Ising model carries a string symmetry. For $V_y > 0$ in Eq. (2) we therefore expect that periodic boundaries along the x direction will lift the degeneracy for finite sized systems. Finite sized corrections to the 2^{L_y} degeneracy are discussed in Ref. [6] for the quantum compass model on periodic boundaries. We therefore use open boundaries along the x direction (cylindrical boundaries) to prevent perturbations to the 2^{L_y} degeneracy due to finite size effects.

In the simulation, we check the convergence of various physical quantities with respect to the expansion cutoff N_{\max} . We find that local quantities such as internal energy, average density, density-density correlation function, etc., converge much faster than the non-local parity operator P at low temperatures, which usually requires a much larger N_{\max} . In practice we find the following values for N_{\max} to be enough for P to converge in our simulations in the desired low temperature range, $N_{\max} = 5000, 8000$, and 10000 for $L = 4, 6$, and 8 , respectively.

Validating a Mean Field Picture

To demonstrate the existence of free Majorana fermions and domains we perform a mean field decoupling of Eq. (2) along the y direction. We then verify the mean field theory (MFT) by direct comparison with an unbiased QMC analysis.

To construct the mean field equations we divide the lattice into 2 sublattices, A and B , along the y direction, and decouple the interaction terms. We obtain the following 4 coupled mean field equations:

$$\begin{aligned} H_1^\alpha &= -8t \langle \tilde{a}_{i,\alpha} \rangle \tilde{a}_{i,\alpha} - \tilde{\mu}_\alpha \left(n_{i,\alpha} - \frac{1}{2} \right), \\ H_2^\alpha &= -t \sum_i \left(a_{i,\alpha}^\dagger - a_{i,\alpha} \right) \left(a_{i+1,\alpha}^\dagger + a_{i+1,\alpha} \right) \\ &\quad - \tilde{\mu}_\alpha \sum_i n_{i,\alpha}, \end{aligned} \quad (9)$$

where $\alpha \in \{A, B\}$ and $\tilde{\mu}_{A/B} = \mu_{A/B} - 2V_y \langle n_{i,B/A} - \frac{1}{2} \rangle$. μ_A and μ_B are chemical potentials for A and B sublattices, and $\tilde{a}_{i,j} \equiv F_{i,j} (a_{i,j}^\dagger + a_{i,j})/2$. The transformation coefficients are given by

$$F_{i,j} = \prod_{j' < j} \prod_k (1 - 2n_{k,j'}) \prod_{i' < i} (1 - 2n_{i',j}), \quad (10)$$

where the summation over j' is extended over all the lattice rows except row j . Note that the operator $\tilde{a}_{i,j}$ corresponds to a spin $\frac{1}{2}$ operator along the x direction in spin space, $S_{i,j}^x$, based on the Jordan-Wigner transformation [1]. In the spin language, the first equation defines a single spin in a magnetic field while the second is a quantum Ising model. We use the solutions of both of these models [4, 5] to solve both models exactly and then the coupled equations, Eqs. (9), through iteration.

Solutions of Eqs. (9) exhibit domains. To see this note that the second Hamiltonian in Eqs. (9), taken by itself, is a one dimensional model demonstrating Majorana fermions [7] at zero temperature. It maps onto the first two terms in Eq. (4). But the first Hamiltonian in Eqs. (9) just enforces a coupling between x -rows. The interchain coupling in the original model Eq. (2) appears as a chemical potential shift in the mean field model defined by Eqs. (9).

Eqs. (9) assume a spatially uniform chemical potential (for each sublattice). If this assumption is correct, it implies that excitations for any given x -row are copied to all other x rows to yield a domain. The existence of domains of string operators is therefore implicit in the mean field theory but we must validate Eq. (9) as a good approximation to Eq. (2) to justify this picture.

We validate Eqs. (9) by direct comparison with QMC solutions to Eq. (2). To compare we compute correlation functions using both MFT and QMC. The following

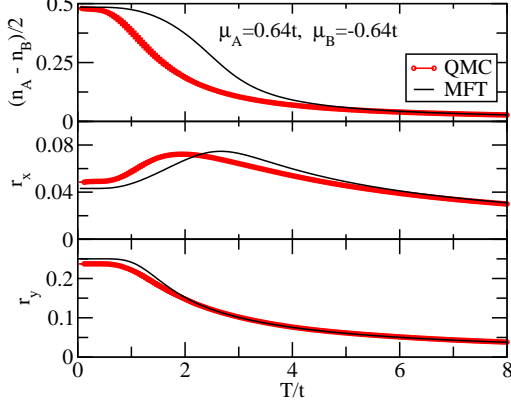


FIG. 5: QMC and MFT comparison of the staggered density (top), intra- x -row hopping and pairing correlation function (middle), and the inter- x -row density-density correlation function (bottom) at $V_y = 4.8t$. We apply staggered chemical potentials μ_A and μ_B to the A and B sublattices, respectively. We choose $L = 4$ for both QMC and MFT calculations.

local correlation functions define quantum bond order along the x direction and classical bond order along the y direction.

$$\begin{aligned} r_x &\equiv \langle (a_{i,j}^\dagger - a_{i,j})(a_{i+1,j}^\dagger + a_{i+1,j}) \rangle, \\ r_y &\equiv \langle (\frac{1}{2} - n_{i,j})(n_{i,j+1} - \frac{1}{2}) \rangle. \end{aligned} \quad (11)$$

Under the spin mapping these correlation functions have been studied in a corresponding spin model, the quantum compass model [8, 9].

Fig. 5 shows that the MFT offers an excellent approximation to the QMC results. The large value of V_y leads to density-wave ordering along y (large r_y). But the non-zero values of r_x show quantum correlations along the x direction. Therefore both QMC and MFT show that the y -columns superpose throughout the lattice to yield a quantum entangled ground state at non-zero temperatures. The good agreement between QMC and MFT therefore supports the domain picture implicit in Eqs. (9).

System-Reservoir Optical Lattice Geometry

We show that an optical superlattice can be used to host a two dimensional “system” lattice parallel to a two dimensional “reservoir” lattice. The system lattice is an array of chains in the $x - y$ plane that allow strong tunneling along the x -direction and weak tunneling along the y -direction. The reservoir lattice is a square lattice with equal tunneling along both the x and y direction.

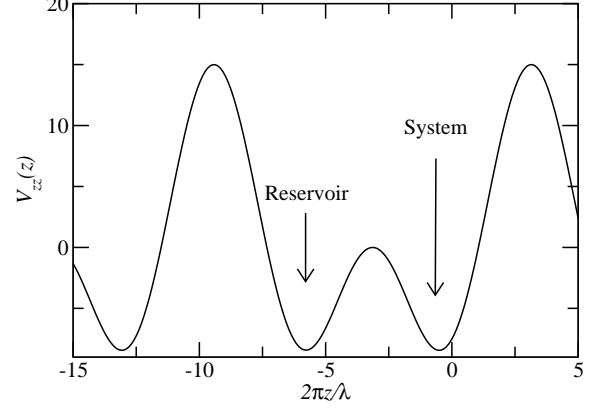


FIG. 6: Plot of the potential defining a double well optical lattice along the z direction for $v_z = -15E_R$, $\phi_1 = 0$, and $\phi_2 = 3\pi/2$.

The increased dimensionality of the reservoir strengthens the pair superfluid in the reservoir. A tunable potential barrier controls the single particle tunneling between the system and the reservoir.

The optical lattice is formed from three laser beam pairs: 1) a double well optical lattice potential, V_{zz} , formed from the interference of counter propagating beams along the z direction, 2) a pair of beams with the same polarization counter-propagating in the x - z plane, to form V_{xz} , and 3) a similar pair of beams but in the y - z plane, to form V_{yz} . If each beam pair does not interfere then the total potential experienced by the particles is: $V_{\text{tot}}(x, y, z) = V_{zz}(z) + V_{xz}(x, z) + V_{yz}(y, z)$.

The system and reservoir are formed from the double well lattice along the z direction. The potential V_{zz} can be formed from the interference of two counter propagating lasers with differing wavelengths (See, e.g., Ref [10]). The distance between the system and the reservoir can be changed by using different laser wavelengths to define the double well. We choose the wavelengths to differ by a factor of 2 to yield:

$$V_{zz}(z) = \frac{v_z}{2} [\cos(kz - \phi_1) - \cos(kz/2 - \phi_2)] \quad (12)$$

Here the wavevector of the primary lattice is $k = 2\pi/\lambda$. This potential is plotted in Fig. 6.

We consider an arrangement where the potential established by the remaining beam pairs is given by:

$$\begin{aligned} V_{xz}(x, z) &= v_x [\cos(kx) + \cos(kz)]^2 \\ V_{yz}(y, z) &= v_y [\cos(ky) + \cos(kz)]^2 \end{aligned} \quad (13)$$

Because the beam pairs forming V_{xz} and V_{yz} each have

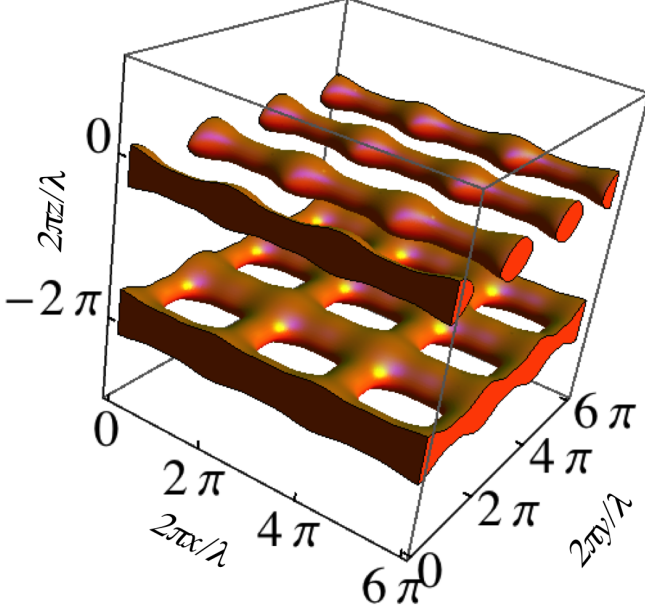


FIG. 7: Plot of the total potential for the system-reservoir optical lattice, V_{tot} . Points are plotted for $v_{\text{tot}} < -10E_R$. The parameters are chosen to be: $v_z = -15E_R$, $v_x = -0.5E_R$, $v_y = -1E_R$, $\phi_1 = -(k\pi + 2\pi/1.9)$, and $\phi_2 = -(k\pi/2 + 2\pi/1.9)$.

the same polarization, they interfere to form a node in the z direction at the location of the reservoir. The reservoir then experiences a nearly isotropic square lattice even with $v_x \neq v_y$.

Fig. 7 plots an equipotential surface defined by V_{tot} . The potentials are defined in units of the lattice recoil,

$E_R \equiv \hbar^2/2m\lambda^2$. Here m is the mass of the particles. Fig. 7 shows a configuration where the particles in the system lattice, near $z = 0$, have little tunneling along y whereas the reservoir lattice, near $z = -\lambda$, is essentially a two-dimensional square lattice. This geometry allows a two-dimensional dipolar superfluid in the reservoir to be placed in close proximity to the system lattice.

-
- [1] Chen, H., Fang, C., Hu, J., and Yao, H., Quantum phase transition in the quantum compass model. *Phys. Rev. B* **75**, 144401 (2007).
 - [2] Syljuasen, O. F. and Sandvik, A. W., Quantum Monte Carlo with directed loops. *Phys. Rev. E* **66**, 046701 (2002).
 - [3] Troyer, M., Wessel, S., and Alet, F., Flat Histogram Methods for Quantum Systems: Algorithms to Overcome Tunneling Problems and Calculate the Free Energy. *Phys. Rev. Lett.* **90**, 120201 (2003).
 - [4] Pfeuty, P., The one-dimensional Ising model with a transverse field. *Ann. Phys.* **57**, 79 (1970).
 - [5] Lieb, E., Schultz, T., and Mattis, D., Two soluble models of an antiferromagnetic chain. *Ann. Phys.* **16**, 407 (1961).
 - [6] Dorier, J., Becca, F., Mila, F., Quantum compass model on the square lattice. *Phys. Rev. B* **72**, 024448 (2005).
 - [7] Kitaev, A. Y., Unpaired Majorana fermions in quantum wires. *Phys.-Usp.* **44**, 131 (2001).
 - [8] Scarola, V. W., Whaley, K. B., and Troyer, M., Thermal canting of spin-bond order. *Phys. Rev. B* **79**, 085113 (2009).
 - [9] Nussinov, Z. and Fradkin, E., Discrete sliding symmetries, dualities, and self-dualities of quantum orbital compass models and p+ip superconducting arrays. *Phys. Rev. B* **71**, 195120 (2005).
 - [10] Foelling, S. *et al.*, Direct observation of second-order atom tunneling. *Nature* **448**, 1029 (2007).